The generalized Mackenzie distribution: disorientation angle distributions for arbitrary textures

The generalized Mackenzie distribution: disorientation angle distributions for arbitrary textures

J.K. Mason and C.A. Schuh†
Department of Materials Science and Engineering
Massachusetts Institute of Technology
Cambridge, MA 02139 USA

Abstract

A general formulation for the disorientation angle distribution function is derived. The derivation employs the hyperspherical harmonic expansion for orientation distributions, and an explicit solution is presented for materials with cubic crystal symmetry and arbitrary textures. The result provides a significant generalization to the well-known Mackenzie distribution function (Mackenzie JK. Biometrika 1958;45:229) for materials with random crystal orientations. This derivation also demonstrates that the relatively new hyperspherical harmonic expansion provides access to results that have been inaccessible with the more traditional 'generalized spherical harmonic' expansion that is in current use throughout the field.

Keywords: texture; grain boundaries; analytical methods

† corresponding author: schuh@mit.edu

1. Introduction

The study of disorientations between neighboring crystals begins, in some sense, with the so-called "Mackenzie distribution" [1], which gives the probability density of observing a particular disorientation angle between randomly oriented cubic crystals. This distribution is one of the simplest and most widely known results involving three-dimensional geometrical probabilities in materials science. While the direct applicability of the Mackenzie distribution is sharply restricted to a small class of microstructures, it is nevertheless frequently used to measure the deviation of experimental disorientation angle distributions from the random case. Such comparisons are useful because the properties and behaviors of grain boundaries are in many cases related to the magnitude of the disorientation angle [2, 3]. The disorientation angle distribution is often used to quantify changes in the grain boundary network resulting from various processing procedures as well [4, 5], and therefore continues to be a function of direct engineering significance.

It is an interesting historical fact that, concurrently with Mackenzie's work, Handscomb [6] developed an analogous solution to the problem using a different mathematical framework. The near-simultaneous appearance of Refs. [1] and [6] suggests that the "Mackenzie distribution" is more aptly named the "Handscomb-Mackenzie distribution", but it also highlights an important theme for the present work. Whereas Mackenzie's derivation proceeded using rotation matrices to describe orientations and misorientations, Handscomb worked in the framework of quaternions. The unique and beneficial properties of the quaternion parameterization led Handscomb to a short and transparent analytical solution in only four pages, whereas the Mackenzie derivation required twelve. A close analogy to this situation is addressed in the present paper, where we consider the generalization of the Handscomb-Mackenzie problem from simple random textures to the case of arbitrary textures. Whereas this problem has remained intractable for the past 50 years when relying on orientation distributions expressed as functions of the Euler angles, by once more exploiting the properties of the quaternion parameterization we are able to achieve an explicit solution.

The Handscomb-Mackenzie function is a distribution of disorientation angles. As such, it is essentially a projection of the more general misorientation distribution function (MDF), which provides the probability of measuring a particular relative misorientation of adjacent grains. Although the literature provides general formulations by which to express an arbitrary orientation distribution function (ODF) or MDF analytically [7], there does not appear to be any means by which to describe the simpler disorientation angle distribution function explicitly. There are only two exceptions of which we are aware. The first exception is the case addressed by Handscomb [6] and Mackenzie [1] for materials with randomly oriented crystals, i.e., for materials with perfectly uniform ODFs. Although their solutions apply specifically for crystals of cubic point symmetry, their approach has more recently been extended to materials of arbitrary crystal symmetry [8, 9]. The second exception is for ensembles of two-dimensional crystals where the only allowed rotations are in the plane of the material, for which disorientation distributions have been derived for some specific textures [10, 11] and for more general families of textures as well [12]. Nevertheless, a general explicit formula for the disorientation angle distribution function that begins from an arbitrary ODF or MDF of an inherently three-dimensional material does not appear to exist. As noted above, we ascribe this to the nature of the current mathematical treatment of the ODF and the MDF.

For historical reasons, the prevailing treatment of orientation information is based on the description of a rotation by Euler angles, and of the ODF and MDF as linear combinations of functions of Euler angles [7]. In principle, the disorientation angle distribution function could be found by expressing the Euler angles as functions of the axis and angle of rotation, substituting these formulas into the existing analytical description of the MDF, and integrating out the axis information. However, the conversion formulas from the Euler angle to the axis-angle description of a rotation are unwieldy enough to effectively preclude the application this method. This purely mathematical obstacle would be removed if, instead of expressing the ODF and MDF as functions of Euler angles and then converting them to the axis-angle description, the ODF and MDF were expanded as linear combinations of functions of the axis and angle of rotation directly. Then the reduction of the MDF to the disorientation angle distribution function would be as simple as integrating out the axis information.

We have recently provided an alternative expansion of the ODF and MDF as linear combinations of functions simply related to the axis-angle description of rotations [13]; we refer to it as the hyperspherical harmonic expansion. As a parallel to the work of Handscomb [6], this expansion is constructed with reference to the unique properties of quaternions. It consequently offers certain advantages and simplifications with regard to the presentation, interpretation, and manipulation of orientation distributions as compared to treatments based on the Euler angles. As a result, the derivation of a general, explicit form for the disorientation angle distribution function is now practicable for the first time. We present this derivation for materials with cubic crystal symmetry in the current paper, along with some related results.

2. Quaternions and the hyperspherical harmonics

A crystal orientation may be described by a rotation operation that brings a reference crystal into coincidence with the actual crystal. Similarly, a misorientation between two crystals may be described by a rotation operation that brings one of the crystals into coincidence with the other. The MDF and ODF therefore share a common mathematical framework as functions describing probability distributions of rotations. The description of rotations followed in this paper is by the triplet of angles ω, θ, and ϕ, where $0 \le \omega \le 2\pi$ is the rotation angle and $0 \le \theta \le \pi$ and $0 \le \phi < 2\pi$ are the spherical angles of the axis of rotation. A rotation is further interpreted as an active rotation of space, rather than as a passive rotation of the coordinate system. The components of a quaternion corresponding to a given rotation may be constructed from these angles by the formulas [14]

$$\begin{aligned} q_0 &= \cos(\omega/2) \\ q_1 &= \sin(\omega/2)\sin\theta\cos\phi \\ q_2 &= \sin(\omega/2)\sin\theta\sin\phi \\ q_3 &= \sin(\omega/2)\cos\theta, \end{aligned} \qquad (1)$$

where the four components satisfy the normalization condition $q_0^2 + q_1^2 + q_2^2 + q_3^2 = 1$, and the word ‘quaternion’ everywhere indicates a normalized quaternion.

The advantage of expressing a rotation in this way is that every normalized quaternion resides on the unit sphere in four dimensions. That is, a collection of three-

dimensional rotations is mapped to a collection of points on the four-dimensional unit sphere. Meanwhile, an arbitrary square-integrable function on the four-dimensional unit sphere may be expanded as an infinite linear combination of harmonic functions restricted to this space. We refer to these functions as the hyperspherical harmonics, and indicate them by the symbol $Z_{l,m}^{n}$. Since the hyperspherical harmonics are defined on the four-dimensional unit sphere, and any point on the four-dimensional unit sphere may be written as functions of the angles ω, θ, and ϕ via Eq. (1), the hyperspherical harmonics may be written as explicit functions of these angles as well [15, 16]:

$$Z_{l,m}^{n}(\omega,\theta,\phi) = (-i)^{l} \frac{2^{l+1/2} l!}{2\pi} \sqrt{(2l+1)\frac{(l-m)!}{(l+m)!}\frac{(n+1)(n-l)!}{(n+l+1)!}} \sin^{l}(\omega/2) C_{n-l}^{l+1}[\cos(\omega/2)] \times P_{l}^{m}(\cos\theta) e^{im\phi}, \quad (2)$$

with integer indices $0 \le n$, $0 \le l \le n$, and $-l \le m \le l$, and where C_{n-l}^{l+1} and P_{l}^{m} stand for a Gegenbauer polynomial and an associated Legendre function, respectively [17, 18]. The hyperspherical harmonics provide a complete, orthonormal basis for the expansion of a square-integrable function *f* on the four-dimensional unit sphere in the form

$$f(\omega,\theta,\phi) = \sum_{n=0,2\ldots}^{\infty} \sum_{l=0}^{n} \sum_{m=-l}^{l} c_{l,m}^{n} Z_{l,m}^{n} . \quad (3)$$

The complex coefficients $c_{l,m}^{n}$ of this expansion may be calculated from the inner product of *f* with the appropriate hyperspherical harmonic $Z_{l,m}^{n}$, or

$$c_{l,m}^{n} = \int_{0}^{2\pi}\int_{0}^{\pi}\int_{0}^{\pi} Z_{l,m}^{n*} f \sin^{2}(\omega/2)\sin\theta d(\omega/2) d\theta d\phi , \quad (4)$$

where * indicates the complex conjugate. Using the above equations, the ODF and MDF may be expressed as analytic functions of quantities relating directly to the axis-angle description of a rotation. While this analysis is described in more detail elsewhere [13], the formulas provided above will be sufficient for the present purpose.

3. The disorientation angle distribution function

The procedure for calculating the disorientation angle distribution function followed in this section requires that the MDF be known. Generally, the MDF is calculated by analyzing the spatial variations of local crystallographic orientation in the

microstructure, using, for example electron back-scatter diffraction data. If the necessary spatial information is not available, then an approximation to the MDF (referred to as the "uncorrelated MDF") may be found from the ODF by means of the procedure provided in Appendix A. The present section further assumes that the MDF is written as an expansion over the complex hyperspherical harmonics, as in Eq. (3). If the MDF is instead written as an expansion over the real or symmetrized hyperspherical harmonics (defined elsewhere [13]), then this expansion may be converted into the form of Eq. (3) by means of the conversion formulas provided in Appendix B. If the MDF is written as an expansion over the generalized spherical harmonics, then the conversion formulas available in the literature [19] may be used to bring the MDF into the required form. Hence, the expansion of the misorientation distribution function M is given by

$$M(\omega,\theta,\phi) = \sum_{n=0,2\ldots}^{\infty} \sum_{l=0}^{n} \sum_{m=-l}^{l} m_{l,m}^{n} Z_{l,m}^{n} \,. \tag{5}$$

Generally speaking, the disorientation angle distribution function, $p(\omega)$, is found from M by integrating over the angular coordinates relating to the axis information, or

$$p(\omega) = \int_{\Omega(\omega)} \sum_{n} \sum_{l} \sum_{m} m_{l,m}^{n} Z_{l,m}^{n} d\Omega \,, \tag{6}$$

where $d\Omega = \sin^2(\omega/2)\sin\theta d\theta d\phi$. Substitution of Eq. (2) into Eq. (6) gives

$$p(\omega) = \sum_{n} \sum_{l} \sum_{m} m_{l,m}^{n} (-i)^l 2^l l! \sqrt{\frac{2}{\pi} \frac{(n+1)(n-l)!}{(n+l+1)!}} \sin^l(\omega/2) C_{n-l}^{l+1}[\cos(\omega/2)] \int_{\Omega(\omega)} Y_l^m(\theta,\phi) d\Omega \,, \tag{7}$$

leaving just the specification of the limits of integration $\Omega(\omega)$, and where Y_l^m is one of the spherical harmonics describing the distribution of rotation axes. Since this depends on the disorientation space of the MDF and therefore on the point symmetry group of the crystallites, Eq. (7) is the simplest presentation of the disorientation angle distribution function for arbitrary materials.

4. Solution for cubic crystals

Given that many engineering materials exhibit cubic point group symmetry, we derive a more explicit formula for the disorientation angle distribution function for this case in the following. The orientation space, or the region within the quaternion group

space containing one point for every unique orientation of a cubic crystal, is defined by the relations [20, 21]

$$\left(\sqrt{2}-1\right)q_0 \geq \pm q_i$$
$$q_0 \geq \pm q_1 \pm q_2 \pm q_3 \qquad (8)$$

where the subscript *i* stands for 1, 2, or 3. The disorientation space, or the region within the quaternion group space containing one point for every unique relative orientation of a pair of cubic crystals, is defined from the orientation space by an additional restriction placed on the allowable rotation axes. This restriction is written as [20, 21]

$$q_1 \geq q_2 \geq q_3 \geq 0\,. \qquad (9)$$

While relations among the four quaternion components are convenient for describing the boundaries of the orientation and disorientation spaces mathematically, relations among three of the components are more suitable for the visualization of these regions. The normalization condition on the four quaternion components may be used to eliminate q_0 from Eqs. (8) and (9), and the resulting formulas give the description of the orientation and disorientation spaces used to construct Fig. 1. This procedure is sometimes referred to as an orthographic projection of the orientation and disorientation spaces from the quaternion space. (Alternatively, a gnomic projection of the orientation and disorientation spaces from the quaternion space returns the analogous figures in the Rodrigues space [22]; this explains the similarity of Fig. 1 to the more well-known view of the orientation space constructed in terms of Rodrigues vectors.).

Equation (1) indicates that the distance of a point from the origin in Fig. (1) is $\sin(\omega/2)$, meaning that a surface of constant ω is a sphere in this space. Returning to Eq. (7), we find that the integration should be performed over the area of intersection of the disorientation space with a sphere of radius $\sin(\omega/2)$ centered at the identity, where the disorientation space is used to avoid the inclusion of multiple symmetrically equivalent regions. Nevertheless, given that the disorientation space is defined from the orientation space by a restriction placed on the axis of rotation, and that the integral in Eq. (7) removes the dependence on the axis of rotation anyway, performing the integration over the area of intersection of the sphere with the orientation space rather than the disorientation space changes $p(\omega)$ by nothing more than a multiplicative constant. The

advantage of using the orientation space instead of the disorientation space is that this choice simplifies the formulas for $p(\omega)$.

An inspection of Fig. 1 indicates that the area of intersection of the orientation space with a sphere centered at the identity is a piecewise function of ω. While the appropriate intervals of ω may be calculated from Eq. (8), the relevant calculations have been reported in detail by other authors [1, 6, 9]. We describe the intervals of ω with reference to Fig. 1 by visualizing the interaction of the boundary of the orientation space with an expanding sphere of radius $\sin(\omega/2)$ centered at the origin.

i. If $0 \le \tan(\omega/2) \le \sqrt{2}-1$, then the sphere is contained within the orientation space. At the upper limit of this region, the sphere contacts the centers of the six octagonal faces.

ii. If $\sqrt{2}-1 \le \tan(\omega/2) \le \sqrt{3}/3$, then spherical caps extend beyond each octagonal face. At the upper limit of this region, the sphere contacts the centers of the eight triangular faces.

iii. If $\sqrt{3}/3 \le \tan(\omega/2) \le 2-\sqrt{2}$, then spherical caps extend beyond each triangular face as well. At the upper limit of this region, the spherical caps extending beyond each face contact the spherical caps of neighboring faces at the center of the shared edges.

iv. If $2-\sqrt{2} \le \tan(\omega/2) \le \sqrt{23-16\sqrt{2}}$, then the spherical caps extending beyond each face overlap with the spherical caps of the neighboring faces. At the upper limit of this region, the sphere contains the entire orientation space.

The area of integration in Eq. (7) and the disorientation angle distribution function $p(\omega)$ must be evaluated independently for each of these intervals of ω.

For the first interval (*i*) of ω, the integration in Eq. (7) is performed over the entire ranges of the angles θ and ϕ. The integral is found to be

$$\sin^2(\omega/2)\int_0^{2\pi}\int_0^{\pi} Y_l^m(\theta,\phi)\sin\theta\, d\theta\, d\phi = 2\sqrt{\pi}\sin^2(\omega/2)\delta_{l,0}\delta_{m.0} \tag{10}$$

by the orthonormality of the spherical harmonics. Substitution of this result into Eq. (7) gives

$$p_1(\omega) = 2\sqrt{2}\sum_n m_{0,0}^n \sin^2(\omega/2) C_n^1[\cos(\omega/2)] \tag{11}$$

for the disorientation angle distribution function in the first interval of ω.

For the second interval (*ii*) of ω, the integration in Eq. (7) is performed over the entire sphere except for the six spherical caps extending beyond octagonal faces. Evaluation of Eq. (7) over this area is equivalent to the result found by subtracting from Eq. (11) the contribution from the area subtended by the spherical caps. By the symmetry of the MDF, the contribution of any one of these spherical caps is identical to that for any other. Therefore, the formula for the disorientation angle distribution function in this interval is found by subtracting from Eq. (11) six times the result S_1 of evaluating Eq. (7) over the spherical cap extending beyond the face in the positive q_3 direction in Fig. 1, or

$$p_2(\omega) = p_1(\omega) - 6S_1(\omega). \tag{12}$$

This spherical cap is defined from Eq. (8) by $\left(\sqrt{2}-1\right)q_0 \le q_3$, which provides the integration limits $0 \le \theta \le \cos^{-1}\left[\left(\sqrt{2}-1\right)\cot(\omega/2)\right]$ with reference to Eq. (1). Meanwhile, the solid angle subtended by the spherical cap includes the entire range of ϕ. Writing $\theta_1(\omega)$ for the upper limit of θ, the relevant integral is then

$$\sin^2(\omega/2)\int_0^{2\pi}\int_0^{\theta_1(\omega)} Y_l^m(\theta,\phi)\sin\theta d\theta d\phi = \sqrt{(2l+1)\pi}\sin^2(\omega/2)\delta_{m.0}\int_{\cos[\theta_1(\omega)]}^1 P_l(x)dx, \tag{13}$$

where the change of variable $x = \cos\theta$ has been performed. The integral over *x* may be evaluated for a lower limit of $\cos\theta$ as

$$\int_{\cos(\theta)}^1 P_l(x)dx = \begin{cases} 1-\cos\theta & l = 0 \\ \sin(\theta)P_l^{-1}(\cos\theta) & l \ne 0 \end{cases}, \tag{14}$$

though we consider the form in Eq. (13) to be simpler from a notational standpoint. Substitution of Eq. (13) into Eq. (7) gives

$$S_1(\omega) = \sqrt{2}\sin^2(\omega/2)\sum_n\sum_l m_{l,0}^n(-i)^l 2^l l!\sqrt{(2l+1)\frac{(n+1)(n-l)!}{(n+l+1)!}}\sin^l(\omega/2)C_{n-l}^{l+1}[\cos(\omega/2)]$$
$$\times \int_{\cos[\theta_1(\omega)]}^1 P_l(x)dx. \tag{15}$$

The solution for $p(\omega)$ in the second interval of ω is then given by direct substitution of Eq. (15) into Eq. (12).

For the third interval (*iii*) of ω, by similar reasoning, the contribution from the eight spherical caps extending beyond triangular faces must be subtracted from Eq. (12). Since there are eight of these spherical caps, and by the symmetry of the MDF they all make the same contribution S_2 to Eq. (7), the disorientation angle distribution function is

$$p_3(\omega) = p_1(\omega) - 6S_1(\omega) - 8S_2(\omega) \tag{16}$$

in the third interval of ω.

To evaluate S_2, we select the spherical cap extending beyond the triangular face in the positive octant of Fig. 1. Since the integrand appearing in Eq. (7) is a spherical harmonic, the symmetry of the spherical cap may be exploited to simplify the integration by initially performing a three-dimensional rotation $R(\omega',\theta',\phi')$ of the integrand to bring the point corresponding to the triangular face's center into coincidence with a point corresponding to the q_3-axis in Fig. 1. The rotation of a spherical harmonic is generally performed by writing the rotated spherical harmonic $R(\omega',\theta',\phi')Y_l^m(\theta,\phi)$ as a linear combination of spherical harmonics with the same value of *l*, or [14]

$$R(\omega',\theta',\phi')Y_l^m(\theta,\phi) = \sum_{m'=-l}^{l} Y_l^{m'}(\theta,\phi)U_{m',m}^l(\omega',\theta',\phi'). \tag{17}$$

The matrix $U_{m',m}^l$ is one of the (2*l*+1)-dimensional irreducible representatives of *SO*(3) [23], while ω', θ' and ϕ' indicate the angle and axis of the rotation being performed. In this case, the arguments of the irreducible representative are determined by the initial coordinates of the triangular face's center. From Eq. (8), this face is defined by the equation $q_0 = q_1 + q_2 + q_3$, which becomes $\cot(\omega/2) = (\sin\phi + \cos\phi)\sin\theta + \cos\theta$ with reference to Eq. (1). Since the center is the point on this face closest to the origin, minimizing ω with respect to θ and ϕ gives $\phi = \pi/4$ and $\theta = \cos^{-1}(\sqrt{3}/3)$ for the angular coordinates of the center point. Therefore, the appropriate values for the arguments ω', θ' and ϕ' of the irreducible representative are $\cos^{-1}(\sqrt{3}/3)$, $\pi/2$, and $7\pi/4$, respectively.

We now require the solid angle subtended by the spherical cap in the rotated position. The equation for the rotated triangular face must be of the same form as the

equation for the octagonal face in the positive q_3 direction, but modified to reflect the increased distance of the triangular face from the origin. These considerations give $\left(\sqrt{3}/3\right)q_0 \le q_3$ for the equation of the rotated face, or $0 \le \theta \le \cos^{-1}\left[\left(\sqrt{3}/3\right)\cot\left(\omega/2\right)\right]$ with reference to Eq. (1). Meanwhile, the integration is performed over the entire range of ϕ. On substituting Eq. (17) for the integrand in Eq. (7) and writing $\theta_2(\omega)$ for the upper limit of θ, the integral in Eq. (7) over the rotated spherical cap is found to be

$$\sin^2\left(\omega/2\right)\int_0^{2\pi}\int_0^{\theta_2(\omega)}\sum_{m'=-l}^{l} Y_l^{m'}(\theta,\phi)U_{m',m}^{l}\left[\cos^{-1}\left(\sqrt{3}/3\right),\pi/2,7\pi/4\right]\sin\theta d\theta d\phi$$

$$= \sqrt{(2l+1)\pi}\sin^2\left(\omega/2\right)U_{0,m}^{l}\left[\cos^{-1}\left(\sqrt{3}/3\right),\pi/2,7\pi/4\right]\int_{\cos[\theta_2(\omega)]}^{1} P_l(x)dx\,, \qquad (18)$$

where the factor of $\delta_{m'.0}$ arising from integration over the complete range of ϕ causes all but one term of the summation over m' to vanish. Applying Eq. (18) to Eq. (7) gives

$$S_2(\omega) = \sqrt{2}\sin^2\left(\omega/2\right)\sum_n\sum_l\sum_m m_{l,m}^{n}(-i)^l 2^l l!\sqrt{(2l+1)\frac{(n+1)(n-l)!}{(n+l+1)!}}\sin^l\left(\omega/2\right)$$

$$\times C_{n-l}^{l+1}\left[\cos\left(\omega/2\right)\right]U_{0,m}^{l}\left[\cos^{-1}\left(\sqrt{3}/3\right),\pi/2,7\pi/4\right]\int_{\cos[\theta_2(\omega)]}^{1} P_l(x)dx \qquad (19)$$

for the contribution that must be subtracted from the disorientation angle distribution function to account for a single spherical cap extending beyond a triangular face. Substitution into Eq. (16) now gives the solution for the third interval of ω.

Finally, for the fourth interval (*iv*) of ω, the contribution from the six spherical caps extending beyond octagonal faces and the eight spherical caps extending beyond triangular faces must still be removed, but with a correction to account for the area excluded twice by the overlap of neighboring spherical caps. Two distinct types of these regions occur, one typified by the area common to the spherical caps extending beyond the neighboring octagonal faces in the positive q_1 and positive q_2 directions in Fig. 1, and the other by the area common to the spherical caps extending beyond the octagonal face in the positive q_3 direction and the triangular face in the positive octant of Fig. 1. By the symmetry of the MDF, the contribution T_1 from first of these regions is symmetrically equivalent to the contribution from any of the overlaps at the twelve edges joining neighboring octagonal faces, while the contribution T_2 from the second of these regions

is symmetrically equivalent to the contribution from any of the overlaps at the twenty-four edges joining neighboring octagonal and triangular faces. Accordingly, the disorientation angle distribution function is written as

$$p_4(\omega) = p_1(\omega) - 6S_1(\omega) - 8S_2(\omega) + 12T_1(\omega) + 24T_2(\omega) \tag{20}$$

in the fourth interval of ω.

Consider the overlap of the spherical caps extending beyond the octagonal faces in the positive q_1 and positive q_2 directions first. From Eq. (8), the equations defining these spherical caps are $\left(\sqrt{2}-1\right)q_0 \le q_1$ and $\left(\sqrt{2}-1\right)q_0 \le q_2$, respectively. With reference to Eq. (1), these become $\left(\sqrt{2}-1\right)\cot(\omega/2) \le \sin\theta\cos\phi$ and $\left(\sqrt{2}-1\right)\cot(\omega/2) \le \sin\theta\cos\phi$. The limits of ϕ may be found as functions of θ by solving the equations of the spherical caps for ϕ, which gives $\sin^{-1}\left[\left(\sqrt{2}-1\right)\cot(\omega/2)\csc\theta\right] \le \phi \le \cos^{-1}\left[\left(\sqrt{2}-1\right)\cot(\omega/2)\csc\theta\right]$. Meanwhile, inspection of Fig. 1 indicates that the maximum and minimum values of θ occur within the overlap region at $\phi = \pi/4$. Inserting this value for ϕ and solving for θ gives $\sin^{-1}\left[\left(2-\sqrt{2}\right)\cot(\omega/2)\right] \le \theta \le \pi - \sin^{-1}\left[\left(2-\sqrt{2}\right)\cot(\omega/2)\right]$ for the limits of θ. These limits may now be used to evaluate Eq. (7) over the area common to a pair of spherical caps on neighboring octagonal faces, with the result

$$T_1(\omega) = \sqrt{2/\pi}\sin^2(\omega/2)\sum_n\sum_l\sum_m m_{l,m}^n(-i)^l 2^l l!\sqrt{\frac{(n+1)(n-l)!}{(n+l+1)!}}\sin^l(\omega/2)C_{n-l}^{l+1}(\cos(\omega/2)) \times \int_{\theta_3(\omega)}^{\theta_4(\omega)}\int_{\phi_1(\omega,\theta)}^{\phi_2(\omega,\theta)} Y_l^m(\theta,\phi)\,d\phi\sin\theta\,d\theta, \tag{21}$$

where $\phi_2(\omega,\theta)$ and $\phi_1(\omega,\theta)$ stand for the upper and lower limits of ϕ, and $\theta_4(\omega)$ and $\theta_3(\omega)$ stand for the upper and lower limits of θ, respectively.

As for the overlap of the spherical caps beyond the octagonal face in the positive q_3 direction and the triangular face in the positive octant, Eq. (8) indicates that these spherical caps are defined by the equations $\left(\sqrt{2}-1\right)q_0 \le q_3$ and $q_0 \le q_1 + q_2 + q_3$, respectively. Reference to Eq. (1) allows these to be written in angular coordinates as $\left(\sqrt{2}-1\right)\cot(\omega/2) \le \cos\theta$ and $\cot(\omega/2) \le \cos\theta + \sqrt{2}\sin\theta\cos(\phi - \pi/4)$. The limits of ϕ may be found as functions of θ by solving this second equation for ϕ, which gives

$$\pi/4-\cos^{-1}\left\{\left[\cot(\omega/2)\csc\theta-\cot\theta\right]/\sqrt{2}\right\}\le\phi\le\cos^{-1}\left\{\left[\cot(\omega/2)\csc\theta-\cot\theta\right]/\sqrt{2}\right\}+\pi/4\,.$$

As before, inspection of Fig. 1 indicates that the maximum and minimum values of θ occur within the overlap region at $\phi=\pi/4$. Inserting this value for ϕ and solving for θ gives $\cos^{-1}\left(\sqrt{3}/3\right)-\cos^{-1}\left[\sqrt{3}\cot(\omega/2)/3\right]\le\theta\le\cos^{-1}\left[\left(\sqrt{2}-1\right)\cot(\omega/2)\right]$ for the limits of θ. With the boundary of the area shared by these neighboring spherical caps defined in angular coordinates, Eq. (7) is evaluated to determine the contribution from this region of overlap as

$$T_2(\omega)=\sqrt{2/\pi}\sin^2(\omega/2)\sum_n\sum_l\sum_m m_{l,m}^n(-i)^l 2^l l!\sqrt{\frac{(n+1)(n-l)!}{(n+l+1)!}}\sin^l(\omega/2)C_{n-l}^{l+1}(\cos(\omega/2))$$
$$\times\int_{\theta_5(\omega)}^{\theta_6(\omega)}\int_{\phi_3(\omega,\theta)}^{\phi_4(\omega,\theta)}Y_l^m(\theta,\phi)d\phi\sin\theta d\theta\,, \qquad (22)$$

where $\phi_4(\omega,\theta)$ and $\phi_3(\omega,\theta)$ stand for the upper and lower limits of ϕ, and $\theta_6(\omega)$ and $\theta_5(\omega)$ stand for the upper and lower limits of θ, respectively.

Unfortunately, there does not appear to be any means to evaluate the integrals appearing in Eqs. (21) and (22) in closed form, and we resort to numerical integration methods. Nevertheless, since the contributions from the overlapping regions are given in an explicit form, we are able to write the disorientation angle distribution function explicitly as well, by introducing Eqs. (21) and (22) into Eq. (20).

This completes the derivation of the explicit form for the disorientation angle distribution function for materials with cubic crystal symmetry. The disorientation angle distribution function $p(\omega)$ is defined in a piecewise fashion, with the solutions in the four distinct intervals of ω given by Eqs. (11), (12), (16), and (20). Although not normalized in the form given above, we now derive the normalization factor for $p(\omega)$. Since the MDF is a probability distribution function, this must be a normalized quantity, or

$$1=\int_0^{2\pi}\int_0^{\pi}\int_0^{\pi}M(\omega,\theta,\phi)\sin^2(\omega/2)\sin\theta d(\omega/2)d\theta d\phi\,. \qquad (23)$$

The cubic point group contains twenty-four elements, meaning that there are forty-eight points in the quaternion space that are symmetrically equivalent to the identity (antipodal pairs of quaternions represent identical rotations) and a corresponding forty-eight regions

that are symmetrically equivalent to the orientation space. Making use of the notation in Eq. (6), this allows Eq. (23) to be written as

$$1 = 48 \int_0^{\omega_{\max}/2} \int_{\Omega(\omega)} M(\omega,\theta,\phi) d\Omega d(\omega/2) = 48 \int_0^{\omega_{\max}/2} p(\omega) d(\omega/2), \tag{24}$$

where $\omega_{\max}$ is the largest rotation angle contained in the orientation space. If $p(\omega)d\omega$ is considered as the probability of sampling a disorientation angle in the range $d\omega$, then Eq. (24) is more conveniently written in the form

$$1 = 24 \int_0^{\omega_{\max}} p(\omega) d\omega, \tag{25}$$

which indicates that multiplying the formulas for $p_i(\omega)$ derived above by a factor of 24 is sufficient to ensure normalization.

5. Solution for random grain orientations

For a material with completely random grain orientations (and no correlations in grain orientations), the misorientations relating neighboring grains will be completely random as well. The MDF for this type of material is therefore uniform. This MDF may be expanded by Eq. (5), with the result that all the expansion coefficients vanish except for $m_{0,0}^0 = 1/\sqrt{2}\pi$. Hence, the comparison of the results of Sec. 4 with the Handscomb-Mackenzie distribution for random textures is in principle as simple as evaluating our formulas for these coefficients and comparing the result to that given in the literature [1, 6]. For convenience, we apply the normalization constraint to the disorientation angle distribution functions in this section.

For the first interval of ω, the formula for the disorientation angle distribution function is given by Eq. (11). Substitution of the appropriate coefficients causes all of the terms in the summation to vanish except for $n = 0$, or

$$p_1(\omega) = 48\sqrt{2}\frac{1}{\sqrt{2}\pi}\sin^2(\omega/2) C_0^1[\cos(\omega/2)]. \tag{26}$$

Simplifying Eq. (26) and recognizing that $C_0^n = 1$ allows this to be written as

$$p_1(\omega) = \frac{48}{\pi}\sin^2(\omega/2) = \frac{24}{\pi}(1-\cos\omega) \tag{27}$$

in the first interval of ω, which is identical to the known result.

For the second interval of ω, the formula for the disorientation angle distribution function is given by introducing Eq. (15) into Eq. (12). Substitution of the appropriate coefficients causes all of the terms in the summations to vanish except for $n = 0$ and $l = 0$, or

$$p_2(\omega) = \frac{24}{\pi}(1-\cos\omega) - 148\sqrt{2}\sin^2(\omega/2)\frac{1}{\sqrt{2}\pi}C_0^1[\cos(\omega/2)]\int_{\cos[\theta_1(\omega)]}^{1} P_l(x)dx\,. \tag{28}$$

Evaluating the integral with reference to Eq. (14) and simplifying the remainder gives

$$p_2(\omega) = \frac{24}{\pi}(1-\cos\omega)\left[3\left(\sqrt{2}-1\right)\cot(\omega/2) - 2\right] \tag{29}$$

in the second interval of ω, which is also identical to the known result.

For the third interval of ω, the formula for the disorientation angle distribution function is found by introducing Eqs. (15) and (19) into Eq. (16). Substitution of the appropriate coefficients causes all of the terms in the summations to vanish except for $n = 0$ and $l = 0$, or

$$p_3(\omega) = \frac{24}{\pi}(1-\cos\omega)\left[3\left(\sqrt{2}-1\right)\cot(\omega/2) - 2\right] - 192\sqrt{2}\sin^2(\omega/2)\frac{1}{\sqrt{2}\pi}C_0^1[\cos(\omega/2)]$$
$$\times U_{0,0}^0\left[\cos^{-1}\left(\sqrt{3}/3\right), \pi/2, 7\pi/4\right]\int_{\cos[\theta_2(\omega)]}^{1} P_l(x)dx\,. \tag{30}$$

The matrix $U_{0,0}^0$, as the irreducible representative of *SO*(3) for a basis of a single element, is identically unity. As before, evaluating the integral with reference to Eq. (14) and simplifying the remainder gives

$$p_3(\omega) = \frac{24}{\pi}(1-\cos\omega)\left\{\left[3\left(\sqrt{2}-1\right) + 4/\sqrt{3}\right]\cot(\omega/2) - 6\right\}. \tag{31}$$

for the disorientation angle distribution function in the third interval of ω, which is identical to the known result.

Finally, we consider the fourth interval of ω. Since there does not appear to be any means to evaluate the integrals in Eqs. (21) and (22) in closed form, even for constant integrands, these formulas do not simplify for the case of uniform texture. However, numerical evaluation of these integrals yields exactly the expected form; in the following section we provide graphical evidence to this effect.

6. Examples of disorientation angle distributions

We apply the above formulas to calculate the disorientation angle distributions for several simulated microstructures with textures of practical interest. We begin by considering simulated materials with cube textures of varying degrees of sharpness, with no spatial correlations among the grains. These materials are constructed by rotating individual crystals from the reference orientation, with any rotation by ω equal to or less than a prescribed threshold angle being equally probable. A set of disorientations is then constructed by sampling many randomly selected pairs of crystals, and subsequently finding a finite expansion of the MDF in the form of Eq. (5). For reference, the {100} pole figures for the textures that were examined are presented in Fig. 2, for several values of the allowed threshold rotation. The corresponding disorientation angle distributions are presented in Fig. 3, where each curve is labeled with the prescribed threshold rotation.

These disorientation angle distributions appear essentially as expected on the basis of physical considerations. Roughly speaking, the ODF of any material of this family is nonzero only within spheres of uniform probability density centered on points in the quaternion space that are symmetrically equivalent to the identity. First consider the material with a threshold rotation angle of 15°. For this material, the boundaries of the spheres of uniform probability density are distant enough that the disorientation angle distribution only contains information relating one part of a given sphere to another part of the same sphere, resulting in a maximum observable disorientation angle of 30°. The situation is similar for a material with a threshold rotation angle of 22.5°, apart from the maximum observable disorientation angle being increased to 45°. For a material with a threshold rotation angle of 30°, the situation is quite different though. The disorientations relating points in neighboring spheres of uniform probability density fall within the disorientation space and make a noticeable contribution to the disorientation angle distribution for large angles. This contribution introduces a marked asymmetry into the peak in probability density that was absent from the disorientation angle distributions of the sharper textures. This behavior becomes more significant for the material with a threshold rotation angle of 37.5°, and for the material with a threshold rotation angle of 45° the spheres of uniform probability density actually make contact with one another (cf.

Fig. 2). While the ODF continues to change as the angular threshold is increased beyond 45°, these changes become less noticeable from the standpoint of the disorientation angle distribution which continues to approach that of a uniform ODF. The heavy dark line in Fig. 3 corresponds to this final disorientation angle distribution as calculated by the method of Sec. 3, and is in perfect agreement with the results of Handscomb [6] and Mackenzie [1].

As expected, the disorientation angle distribution function of all of these textures generally converges to zero at $\omega = 0^\circ$ and $\omega = 62.8^\circ$, since the area of intersection of the orientation space with a sphere of radius $\sin(\omega/2)$ centered at the identity vanishes either when the sphere vanishes or when the sphere extends beyond the orientation space. That this does not always occur at the upper limit of ω in Fig. 3 indicates a potentially significant truncation error or numerical integration round-off error. Meanwhile, the oscillations that are visible for the material with a threshold rotation angle of 15° are clearly due to a truncation error, since they occur outside the region where numerical integration is performed. These sources of error result in areas of unphysical negative probability density, though they may be addressed either by increasing the number of terms in the expansion, or by dealing strictly with textures that do not contain sharp discontinuities that are difficult to capture with a finite-order series expansion (as in the present case where we have prescribed a sharp threshold rotation angle within which all orientations must lie).

Figure 4 shows the disorientation angle distributions for a simulated material and for an experimental material (as measured by Mishin et al. [24]) with strong copper textures, in the absence of correlations relating the orientations of neighboring grains and relating the orientation and shape of a single grain. A comparison of the disorientation angle distributions presented in Fig. 4 is encouraging. Specifically, the experimental result deviates from the reference distribution in the direction of the simulated result, which is expected since the simulated texture is sharper than the experimental one.

7. Conclusion

The disorientation angle distribution is a common and straightforward method to characterize some features of the grain boundary network, and benefits from a marked

simplicity of measurement and presentation in experimental situations. Despite the use of the disorientation angle distribution function in the literature spanning several decades, the authors are aware of analytical formulas reported for this function only for materials where every misorientation of neighboring grains is equally likely [1, 6, 8, 9], or where the problem is restricted to inherently two-dimensional materials [10-12]. We attribute the absence of a more general formulation to certain difficulties inherent to the customary treatment of rotation distributions as linear combinations of the generalized spherical harmonics [7]. In particular, because the generalized spherical harmonics are written as functions of Euler angles, they cannot be easily transcribed into a form permitting analytical separation of rotation axis and angle.

On the other hand, the recently proposed alternative for the expansion of a rotation distribution function as a linear combination of the hyperspherical harmonics [13] is given as a function of quantities relating directly to the axis and angle of rotation. Writing the MDF of a material in this form immediately allows one to find a general, explicit formula for the misorientation angle distribution function, as is provided here in Eq. (7). The current paper applies this formula more specifically to materials with cubic crystal symmetry, for which the misorientation angle distribution function must be defined in a piecewise fashion over four intervals. The explicit solutions in each of these intervals are reported in Eqs. (11), (12), (16), and (20). These expressions reduce properly to the well-known solutions of Mackenzie [1] and Handscomb [6] when grains are randomly oriented, but generalize the result to arbitrary textures.

Acknowledgements

This work was supported by the US National Science Foundation under Contract #DMR-0346848.

References

[1] Mackenzie JK. Second Paper on Statistics Associated with the Random Disorientation of Cubes. Biometrika 1958;45:229.

[2] Hilgenkamp H, Mannhart J. Grain boundaries in high-T-c superconductors. Rev Mod Phys 2002;74:485.
[3] Roberts CG, Semiatin SL, Rollett AD. Particle-associated misorientation distribution in a nickel-base superalloy. Scripta Materialia 2007;56:899.
[4] Dalla Torre FH, Gazder AA, Gu CF, Davies CHJ, Pereloma EV. Grain size, misorientation, and texture evolution of copper processed by equal channel angular extrusion and the validity of the Hall-Petch relationship. Metallurgical and Materials Transactions 2007;38A:1080.
[5] Kang JY, Bacroix B, Regle H, Oh KH, Lee HC. Effect of deformation mode and grain orientation on misorientation development in a body-centered cubic steel. Acta Mater 2007;55:4935.
[6] Handscomb DC. On the Random Disorientation of Two Cubes. Canadian J Math 1957;10:85.
[7] Bunge HJ. Texture analysis in materials science: mathematical methods. Gottingen: Cuvillier Verlag, 1993.
[8] Grimmer H. Distribution of Disorientation Angles If All Relative Orientations of Neighboring Grains Are Equally Probable. Scripta Metall Mater 1979;13:161.
[9] Morawiec A. Misorientation-Angle Distribution of Randomly Oriented Symmetrical Objects. Journal of Applied Crystallography 1995;28:289.
[10] Frary M, Schuh CA. Percolation and statistical properties of low- and high-angle interface networks in polycrystalline ensembles. Phys Rev B 2004;69:134115.
[11] Van Siclen CD. Intergranular fracture in model polycrystals with correlated distribution of low-angle grain boundaries. Phys Rev B 2006;73:184118.
[12] Mason JK, Schuh CA. Correlated grain-boundary distributions in two-dimensional networks. Acta Cryst A 2007;63:315.
[13] Mason JK, Schuh CA. Hyperspherical harmonics for the representation of crystallographic texture. Acta Mater 2008;56:6141.
[14] Altmann SL. Rotations, quaternions, and double groups. Oxford: Clarendon Press, 1986.
[15] Biedenharn LC. Wigner Coefficients for the R4 Group and Some Applications. J Math Phys 1961;2:433.
[16] Bander M, Itzykson C. Group Theory and the Hydrogen Atom (I). Rev Mod Phys 1966;38:330.
[17] Bateman H, Erdélyi A. Higher transcendental functions. New York: McGraw-Hill, 1953.
[18] Gradshtein IS, Ryzhik IM, Jeffrey A. Table of integrals, series, and products. San Diego: Academic Press, 2000.
[19] Mason JK, Schuh CA. Expressing Crystallographic Textures through the Orientation Distribution Function: Conversion between the Generalized Spherical Harmonic and Hyperspherical Harmonic Expansions. under review.
[20] Grimmer H. Disorientations and Coincidence Rotations for Cubic Lattices. Acta Cryst A 1974;30:685.
[21] Heinz A, Neumann P. Representation of Orientation and Disorientation Data for Cubic, Hexagonal, Tetragonal and Orthorhombic Crystals. Acta Cryst A 1991;47:780.
[22] Frank FC. Orientation Mapping. Metall Trans A 1988;19:403.

[23] Mason JK. The Relationship of the Hyperspherical Harmonics to SO(3), SO(4) and the Orientation Distribution Function. Acta Cryst A. Cambridge, MA: Massachusetts Institute of Technology, 2009.
[24] Mishin OV, Gertsman VY, Gottstein G. Distributions of orientations and misorientations in hot-rolled copper. Mater Charact 1997;38:39.
[25] Gertsman VY, Zhilyaev AP, Pshenichnyuk AI, Valiev RZ. Modeling of Grain-Boundary Misorientation Spectrum in Polycrystals with Crystallographic Texture. Acta Metall Et Mater 1992;40:1433.
[26] Garbacz A, Grabski MW. The Relationship between Texture and CSL Boundaries Distribution in Polycrystalline Materials .1. The Grain-Boundary Misorientation Distribution in Random Polycrystal. Acta Metall Et Mater 1993;41:469.
[27] Zhilyaev AP, Gertsman VY, Mishin OV, Pshenichnyuk AI, Aleksandrov IV, Valiev RZ. Grain-Boundary Misorientation Spectra (Gbms) Determined by Real Odf in FCC-Materials Susceptible to Annealing Twinning. Acta Metall Et Mater 1993;41:2657.
[28] Zuo L, Watanabe T, Esling C. A Theoretical Approach to Grain-Boundary-Character-Distribution (GBCD) in Textured Polycrystalline Materials. Zeitschrift Fur Metallkunde 1994;85:554.
[29] Morawiec A, Szpunar JA, Hinz DC. Texture Influence on the Frequency of Occurrence of CSL-Boundaries in Polycrystalline Materials. Acta Metall Et Mater 1993;41:2825.
[30] Zhao J, Adams BL, Morris PR. A Comparison of Measured and Texture-Estimated Misorientation Distributions in Type 304 Stainless Steel Tubing. Texture Microstruct 1988;8 & 9:493.
[31] Bunge HJ, Weiland H. Orientation Correlation in Grain and Phase Boundaries. Texture Microstruct 1988;7:231.

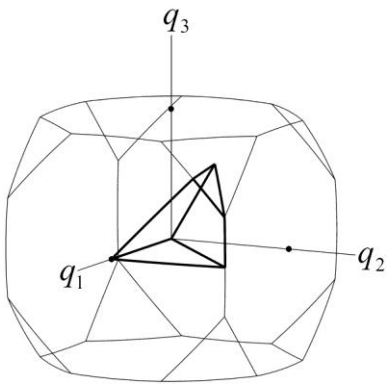

Figure 1: The cubic orientation (light lines) and disorientation (bold lines) spaces, displayed in the orthographic projection of the quaternion space. The solid points mark the intersection of the axes with the surface of the orientation space. The q_i are the components of the vector part of the quaternion.

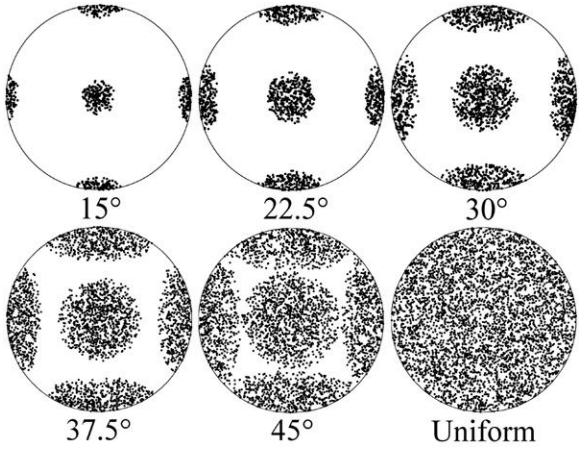

Figure 2: {100} pole figure plots for simulated cube textures of varying degrees of sharpness, plotted in equal area projection. The angles indicate the maximum allowed disorientation angle of a cubic crystal from the reference orientation. The normal direction is out of the page, and the rolling direction is vertical in the plane of the page.

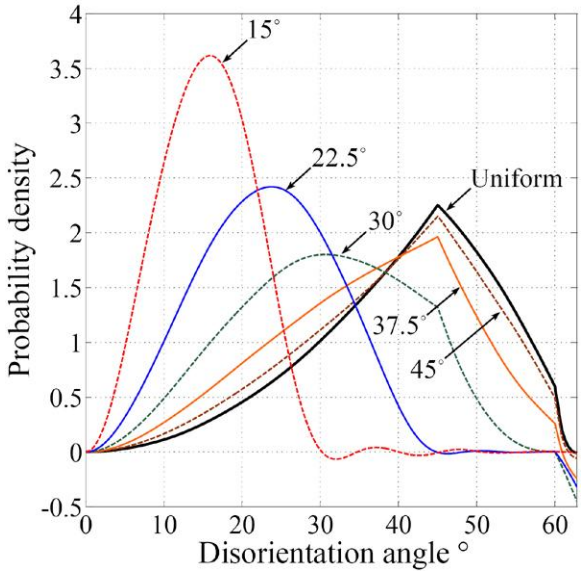

Figure 3: Disorientation angle distribution functions corresponding to simulated cube textures of varying degrees of sharpness (cf. Fig. 2). Labels given in degrees indicate the maximum allowed disorientation angle of a cubic crystal from the reference orientation (smaller values denote sharper textures), while the heavy dark line corresponds to a material in which every misorientation is equally likely.

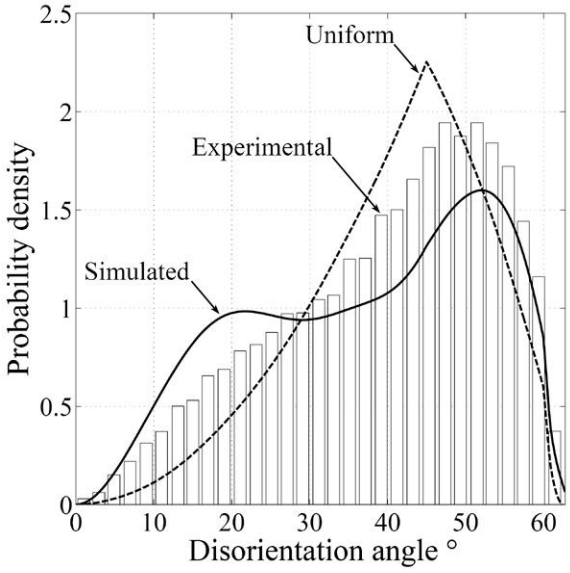

Figure 4: Disorientation angle distribution function for a copper texture, assuming the absence of correlations relating the orientations of neighboring grains or relating the orientation and shape of a single grain. The solid line is the result of our simulation, while the bars indicate the probability density for an experimental material with a similar texture, as measured by Mishin, Gertsman and Gottstein [24]. The dashed line corresponds to a material in which every misorientation is equally likely (i.e., the Mackenzie distribution).

Appendix A: Calculation of the MDF from the ODF

While the MDF of a material is certainly connected to the ODF [25-28], the ODF is not the only contributing factor. The presence of correlations relating the orientations of neighboring grains or correlations relating the orientation and shape of a single grain may have a strong effect on the misorientations present in a material [29]. Nevertheless, if these correlations are assumed absent, then one is able to predict an "uncorrelated MDF" from the ODF alone. Although derivations of the uncorrelated MDF from the ODF within the framework of the generalized spherical harmonic expansion have been presented elsewhere in the literature [30, 31], we present this derivation within the framework of the hyperspherical harmonic expansion for the first time.

Assume that two crystals are in the reference orientation, and that their relative misorientation is described by the identity rotation. Act on the first crystal with the rotation Δg, with the result that the misorientation of the crystals is described by the same Δg. Now, act on the pair of crystals with the further rotation g. The final orientation of the first crystal is described by $g \cdot \Delta g$, where $\cdot$ denotes the rotation multiplication operation with the order of operations running from right to left, and the final orientation of the second crystal is described simply by g. Since the relative misorientation of the crystals is still described by Δg, the relative misorientation is clearly independent of the choice of g. Therefore, the probability density of observing a relative crystal misorientation of Δg is given by the probability density of observing crystals with orientations described by $g \cdot \Delta g$ and g, integrated over all g. That is,

$$M'(\Delta g) = \int f^*(g) f(g \cdot \Delta g) dg \,, \tag{A1}$$

where f is the ODF, M' is the uncorrelated MDF, and * indicates the complex conjugate. Writing f in Eq. (A1) in the form of Eq. (3) gives

$$M'(\Delta g) = \int \sum_{n''} \sum_{n'} \sum_{l''} \sum_{l'} \sum_{m''} \sum_{m'} c_{l'',m''}^{n''*} c_{l',m'}^{n'} Z_{l'',m''}^{n''*}(g) Z_{l',m'}^{n'}(g \cdot \Delta g) dg \,. \tag{A2}$$

Since the integration is only with respect to g, separating the dependence of $Z_{l',m'}^{n'}$ on g and Δg would allow the integral to be evaluated and Eq. (A2) to be simplified. The

desired decomposition of $Z_{l',m'}^{n'}$ is permitted by means of the hyperspherical harmonic addition theorem [23], with the result

$$M'(\Delta g)=\int\sum_{n''}\sum_{n'}\sum_{l''}\sum_{l'}\sum_{m''}\sum_{m'}c_{l'',m''}^{n''*}c_{l',m'}^{n'}Z_{l'',m''}^{n''*}(g)\frac{\sqrt{2}\pi}{\sqrt{n'+1}}\sum_{l'''}\sum_{l}\sum_{m'''}\sum_{m}\sqrt{2l'''+1}\sqrt{2l+1}$$
$$\times(-1)^{-l'''-l}Z_{l''',m'''}^{n'}(g)Z_{l,m}^{n'}(\Delta g)C_{l''',m''',l,m}^{l',m'}\begin{Bmatrix} l' & l''' & l \\ n'/2 & n'/2 & n'/2\end{Bmatrix}dg\,. \qquad \text{(A3)}$$

Collecting the quantities that do not depend on g outside the integral and rearranging the summations yields

$$M'(\Delta g)=\sum_{n'}\sum_{l}\sum_{m}Z_{l,m}^{n'}(\Delta g)\frac{\sqrt{2}\pi}{\sqrt{n'+1}}\sqrt{2l+1}\sum_{n''}\sum_{l'''}\sum_{l''}\sum_{l'}\sqrt{2l'''+1}\begin{Bmatrix} l' & l''' & l \\ n'/2 & n'/2 & n'/2\end{Bmatrix}$$
$$\times(-1)^{-l'''-l}\sum_{m'''}\sum_{m''}\sum_{m'}C_{l''',m''',l,m}^{l',m'}c_{l'',m''}^{n''*}c_{l',m'}^{n'}\int Z_{l'',m''}^{n''*}(g)Z_{l''',m'''}^{n'}(g)dg\,. \qquad \text{(A4)}$$

The integral here is equal to $\delta_{n'',n'}\delta_{l'',l'''}\delta_{m'',m'''}$ by the orthogonality of the hyperspherical harmonics [13], where δ is the Kronecker delta. Simplifying the indices and relabeling the index n' as n gives

$$M'(\Delta g)=\sum_{n}\sum_{l}\sum_{m}Z_{l,m}^{n}(\Delta g)\left[(-1)^{-l}\frac{\sqrt{2}\pi}{\sqrt{n+1}}\sqrt{2l+1}\sum_{l''}\sum_{l'}(-1)^{-l''}\sqrt{2l''+1}\begin{Bmatrix} l' & l'' & l \\ n/2 & n/2 & n/2\end{Bmatrix}\right.$$
$$\left.\times\sum_{m''}\sum_{m'}C_{l'',m'',l,m}^{l',m'}c_{l'',m''}^{n*}c_{l',m'}^{n}\right], \qquad \text{(A5)}$$

where the expression for M' is observed to be in the form of the hyperspherical harmonic expansion of Eq. (3). That is, we may write:

$$M'(\Delta g)=\sum_{n}\sum_{l}\sum_{m}m_{l,m}'^{n}Z_{l,m}^{n}(\Delta g)\,. \qquad \text{(A6)}$$

Comparing Eq. (A5) with Eq. (A6) indicates that

$$m_{l,m}'^{n}=(-1)^{-l}\frac{\sqrt{2}\pi}{\sqrt{n+1}}\sqrt{2l+1}\sum_{l''}\sum_{l'}(-1)^{-l''}\sqrt{2l''+1}\begin{Bmatrix} l' & l'' & l \\ n/2 & n/2 & n/2\end{Bmatrix}\sum_{m''}\sum_{m'}C_{l'',m'',l,m}^{l',m'}c_{l'',m''}^{n*}c_{l',m'}^{n} \qquad \text{(A7)}$$

is the relation determining the expansion coefficients $m_{l,m}'^{n}$ of the uncorrelated MDF from the expansion coefficients $c_{l,m}^{n}$ of the ODF.

Appendix B: Conversions of the hyperspherical harmonic expansion coefficients

Although the majority of the formulas in this paper use a complex version of the hyperspherical harmonic expansion because of the notational simplicity that this affords, the complex version of the expansion is not always the most convenient form. For example, an expansion using the real hyperspherical harmonics and real expansion coefficients is often more suitable for a real-valued function. The real hyperspherical harmonics are defined in terms of the complex hyperspherical harmonics of Eq. (3) as [13]

$$\begin{aligned} Z^n_{l,0,c}(\omega,\theta,\phi) &= (i)^l Z^n_{l,0} \\ Z^n_{l,m,c}(\omega,\theta,\phi) &= (i)^l \left[(-1)^m Z^n_{l,m} + Z^n_{l,-m}\right]/\sqrt{2} \\ Z^n_{l,m,s}(\omega,\theta,\phi) &= (i)^{l-1} \left[(-1)^m Z^n_{l,m} - Z^n_{l,-m}\right]/\sqrt{2}\,, \end{aligned} \tag{B1}$$

where the additional subscript *c* or *s* indicates whether the function is even or odd with respect to ϕ. Explicitly, these functions may be written as

$$\begin{aligned} Z^n_{l,0,c}(\omega,\theta,\phi) &= \frac{2^l l!}{\pi}\sqrt{\frac{(2l+1)}{2}\frac{(n+1)(n-l)!}{(n+l+1)!}}\sin^l(\omega/2)C^{l+1}_{n-l}[\cos(\omega/2)]P_l(\cos\theta) \\ Z^n_{l,m,c}(\omega,\theta,\phi) &= (-1)^m \frac{2^l l!}{\pi}\sqrt{(2l+1)\frac{(l-m)!}{(l+m)!}\frac{(n+1)(n-l)!}{(n+l+1)!}}\sin^l(\omega/2)C^{l+1}_{n-l}[\cos(\omega/2)] \\ &\quad \times P^m_l(\cos\theta)\cos(m\phi) \\ Z^n_{l,m,s}(\omega,\theta,\phi) &= (-1)^m \frac{2^l l!}{\pi}\sqrt{(2l+1)\frac{(l-m)!}{(l+m)!}\frac{(n+1)(n-l)!}{(n+l+1)!}}\sin^l(\omega/2)C^{l+1}_{n-l}[\cos(\omega/2)] \\ &\quad \times P^m_l(\cos\theta)\sin(m\phi)\,. \end{aligned} \tag{B2}$$

The difference in phase of the complex hyperspherical harmonics of Eq. (2) with respect to earlier publications [13] causes a difference in the phase of the real hyperspherical harmonics of Eqs. (B2) as well (cf. Eq. (6) in Ref. [13]). We believe that the current phase of Eq. (2) is preferable to earlier versions though, as is articulated elsewhere [19].

Since the transformation relating the complex hyperspherical harmonics to the real hyperspherical harmonics is linear and invertible, the real hyperspherical harmonics provide an equally suitable basis for the expansion of a rotation distribution function that takes the form of

$$f(\omega,\theta,\phi) = \sum_{n=0,2\ldots}^{\infty}\sum_{l=0}^{n}\left[a^n_{l,0}Z^n_{l,0,c} + \sum_{m=1}^{l}\left(a^n_{l,m}Z^n_{l,m,c} + b^n_{l,m}Z^n_{l,m,s}\right)\right]. \tag{B3}$$

The expansion coefficients of Eq. (B3) may now be defined in terms of the complex expansion coefficients of Eq. (3) by inverting Eqs. (B1), substituting these relations into Eq. (3), and comparing the resulting coefficients with those of Eq. (B3). This gives

$$\begin{aligned} a_{l,0}^{n} &= \left(-i\right)^{l} c_{l,0}^{n} \\ a_{l,m}^{n} &= \left(-i\right)^{l} \left[\left(-1\right)^{m} c_{l,m}^{n} + c_{l,-m}^{n}\right] \Big/ \sqrt{2} \\ b_{l,m}^{n} &= \left(-i\right)^{l-1} \left[\left(-1\right)^{m} c_{l,m}^{n} - c_{l,-m}^{n}\right] \Big/ \sqrt{2}\,, \end{aligned} \tag{B4}$$

corresponding to Eqs. (B1) above. Provided that the function *f* is real-valued, these coefficients will be real as well.

Often, the rotation distribution functions of interest characterize physical systems with certain symmetries. For example, the ODF of a single phase material exhibits the exact point group symmetry of the individual crystallites and the statistical point group symmetry of the arrangement of crystallites within the sample. Accordingly, the expansion of the ODF requires a basis of only those functions that display these symmetries. Roughly, this basis may be constructed by identifying all of the linear combinations of hyperspherical harmonics that satisfy the symmetry conditions and forming an orthonormal set of the linear combinations that span the symmetrized function space. The advantage of an expansion over the symmetrized basis functions is that the use of significantly fewer terms gives a comparable level of accuracy to the more general expansion given in Eq. (3). A description of the calculation of the coefficients of the linear combinations of hyperspherical harmonics that satisfy the symmetry conditions, and the subsequent orthogonalization procedure, is presented elsewhere [13]. The symmetrized basis functions may be written in the form

$$\dddot{Z}_{\lambda}^{n}\left(\omega,\theta,\phi\right) = \sum_{l=0}^{n}\left[\ddot{a}_{\lambda,l,0}^{n} Z_{l,0,c}^{n} + \sum_{m=1}^{l}\left(\ddot{a}_{\lambda,l,m}^{n} Z_{l,m,c}^{n} + \dddot{b}_{\lambda,l,m}^{n} Z_{l,m,s}^{n}\right)\right] \tag{B5}$$

where $\ddot{a}_{\lambda,l,m}^{n}$ and $\dddot{b}_{\lambda,l,m}^{n}$ are the symmetrizing coefficients, which are provided as supplementary content to Ref. [13]. By convention, the triplet of dots above the symmetrizing coefficients and the symmetrized harmonic indicates that the point group symmetries of the crystal and of the sample are both satisfied [7]. Provided that the rotation distribution function *f* displays symmetries equal to or higher than the symmetries of the symmetrized harmonics, the expansion of *f* may be written as

$$f(\omega,\theta,\phi) = \sum_{n=0,2\ldots}^{\infty} \sum_{\lambda=1}^{\Lambda(n)} s_\lambda^n \ddot{\ddot{Z}}_\lambda^n \tag{B6}$$

where $\Lambda(n)$ is the number of symmetrized basis functions for a particular value of n.

While an arbitrary rotation distribution function does not, in general, exhibit the required symmetries and cannot be expanded in the form of Eq. (B6), a rotation distribution function that displays symmetry can certainly be expanded in the more general forms of either Eq. (B3) or Eq. (3). Provided that the expansion coefficients of Eq. (B6) are known, the corresponding expansion coefficients of the more general expansions may easily be found. Substitution of Eq. (B5) into Eq. (B6) and comparison of the result with Eq. (B3) gives

$$\begin{aligned} a_{l,0}^n &= \sum_{\lambda=1}^{\Lambda(n)} s_\lambda^n \ddot{\ddot{a}}_{\lambda,l,0}^n \\ a_{l,m}^n &= \sum_{\lambda=1}^{\Lambda(n)} s_\lambda^n \ddot{\ddot{a}}_{\lambda,l,m}^n \\ b_{l,m}^n &= \sum_{\lambda=1}^{\Lambda(n)} s_\lambda^n \ddot{\ddot{b}}_{\lambda,l,m}^n \end{aligned} \tag{B7}$$

for the coefficients of the corresponding real hyperspherical harmonic expansion. Furthermore, inversion of Eqs. (B4) and substitution of Eqs. (B7) into these relations gives

$$\begin{aligned} c_{l,0}^n &= (i)^l \sum_{\lambda=1}^{\Lambda(n)} s_\lambda^n \ddot{\ddot{a}}_{\lambda,l,0}^n \\ c_{l,m}^n &= (i)^l (-1)^m \sum_{\lambda=1}^{\Lambda(n)} s_\lambda^n \left(\ddot{\ddot{a}}_{\lambda,l,m}^n - i \ddot{\ddot{b}}_{\lambda,l,m}^n \right) \Big/ \sqrt{2} \\ c_{l,-m}^n &= (i)^l \sum_{\lambda=1}^{\Lambda(n)} s_\lambda^n \left(\ddot{\ddot{a}}_{\lambda,l,m}^n + i \ddot{\ddot{b}}_{\lambda,l,m}^n \right) \Big/ \sqrt{2} \end{aligned} \tag{B8}$$

These conversion formulas relate the coefficients of the symmetrized hyperspherical harmonic expansion to the coefficients of the complex hyperspherical harmonic expansion.